UNCOVER: The Growth of the First Massive Black Holes from JWST/NIRSpec—Spectroscopic Redshift Confirmation of an X-Ray Luminous AGN at z = 10.1

The Astrophysical Journal Letters, 955:L24 (8pp), 2023 September 20 https://doi.org/10.3847/2041-8213/acf7c5

UNCOVER: The Growth of the First Massive Black Holes from JWST/NIRSpec—Spectroscopic Redshift Confirmation of an X-Ray Luminous AGN at $z = 10.1$

Andy D. Goulding[1], Jenny E. Greene[1], David J. Setton[2], Ivo Labbe[3], Rachel Bezanson[2], Tim B. Miller[4,5], Hakim Atek[6], Ákos Bogdán[7], Gabriel Brammer[8], Iryna Chemerynska[6], Sam E. Cutler[9], Pratika Dayal[10], Yoshinobu Fudamoto[11,12], Seiji Fujimoto[13,28], Lukas J. Furtak[14], Vasily Kokorev[15], Gourav Khullar[2], Joel Leja[16,17,18], Danilo Marchesini[19], Priyamvada Natarajan[4,20,21], Erica Nelson[22], Pascal A. Oesch[8,23], Richard Pan[24], Casey Papovich[25,26], Sedona H. Price[2], Pieter van Dokkum[4], Bingjie Wang (王冰洁)[16,17,18], John R. Weaver[9], Katherine E. Whitaker[9,27], and Adi Zitrin[14]

[1] Department of Astrophysical Sciences, Princeton University, Princeton, NJ 08544, USA; goulding@astro.princeton.edu
[2] Department of Physics and Astronomy and PITT PACC, University of Pittsburgh, Pittsburgh, PA 15260, USA
[3] Centre for Astrophysics and Supercomputing, Swinburne University of Technology, Melbourne, VIC 3122, Australia
[4] Department of Astronomy, Yale University, New Haven, CT 06511, USA
[5] Center for Interdisciplinary Exploration and Research in Astrophysics (CIERA) and Department of Physics and Astronomy, Northwestern University, 1800 Sherman Ave., Evanston IL 60201, USA
[6] Institut d'Astrophysique de Paris, CNRS, Sorbonne Université, 98bis Boulevard Arago, F-75014, Paris, France
[7] Center for Astrophysics | Harvard & Smithsonian, 60 Garden Street, Cambridge, MA 02138, USA
[8] Cosmic Dawn Center (DAWN), Niels Bohr Institute, University of Copenhagen, Jagtvej 128, København N, DK-2200, Denmark
[9] Department of Astronomy, University of Massachusetts, Amherst, MA 01003, USA
[10] Kapteyn Astronomical Institute, University of Groningen, 9700 AV Groningen, The Netherlands
[11] Waseda Research Institute for Science and Engineering, Faculty of Science and Engineering, Waseda University, 3-4-1 Okubo, Shinjuku, Tokyo 169-8555, Japan
[12] National Astronomical Observatory of Japan, 2-21-1, Osawa, Mitaka, Tokyo, Japan
[13] Department of Astronomy, The University of Texas at Austin, Austin, TX 78712, USA
[14] Physics Department, Ben-Gurion University of the Negev, P.O. Box 653, Beer-Sheva 84105, Israel
[15] Kapteyn Astronomical Institute, University of Groningen, P.O. Box 800, 9700AV Groningen, The Netherlands
[16] Department of Astronomy & Astrophysics, The Pennsylvania State University, University Park, PA 16802, USA
[17] Institute for Computational & Data Sciences, The Pennsylvania State University, University Park, PA 16802, USA
[18] Institute for Gravitation and the Cosmos, The Pennsylvania State University, University Park, PA 16802, USA
[19] Physics and Astronomy Department, Tufts University, 574 Boston Ave., Medford, MA 02155, USA
[20] Department of Physics, Yale University, New Haven, CT 06520, USA
[21] Black Hole Initiative, Harvard University, 20 Garden Street, Cambridge, MA 02138, USA
[22] Department for Astrophysical and Planetary Science, University of Colorado, Boulder, CO 80309, USA
[23] Department of Astronomy, University of Geneva, Chemin Pegasi 51, 1290 Versoix, Switzerland
[24] Department of Physics and Astronomy, Tufts University, 574 Boston Ave., Medford, MA 02155, USA
[25] Department of Physics and Astronomy, Texas A&M University, College Station, TX, 77843-4242 USA
[26] George P. and Cynthia Woods Mitchell Institute for Fundamental Physics and Astronomy, Texas A&M University, College Station, TX, 77843-4242 USA
[27] Cosmic Dawn Center (DAWN), Denmark
Received 2023 August 7; revised 2023 August 31; accepted 2023 September 1; published 2023 September 22

Abstract

The James Webb Space Telescope is now detecting early black holes (BHs) as they transition from "seeds" to supermassive BHs. Recently, Bogdan et al. reported the detection of an X-ray luminous supermassive BH, UHZ-1, with a photometric redshift at $z > 10$. Such an extreme source at this very high redshift provides new insights on seeding and growth models for BHs given the short time available for formation and growth. Harnessing the exquisite sensitivity of JWST/NIRSpec, here we report the spectroscopic confirmation of UHZ-1 at $z = 10.073 \pm 0.002$. We find that the NIRSpec/Prism spectrum is typical of recently discovered $z \approx 10$ galaxies, characterized primarily by star formation features. We see no clear evidence of the powerful X-ray source in the rest-frame UV/optical spectrum, which may suggest heavy obscuration of the central BH, in line with the Compton-thick column density measured in the X-rays. We perform a stellar population fit simultaneously to the new NIRSpec spectroscopy and previously available photometry. The fit yields a stellar-mass estimate for the host galaxy that is significantly better constrained than prior photometric estimates ($M_\star \sim 1.4^{+0.3}_{-0.4} \times 10^8\ M_\odot$). Given the predicted BH mass ($M_{\rm BH} \sim 10^7$–$10^8\ M_\odot$), the resulting ratio of $M_{\rm BH}/M_\star$ remains 2 to 3 orders of magnitude higher than local values, thus lending support to the heavy seeding channel for the formation of supermassive BHs within the first billion years of cosmic evolution.

Unified Astronomy Thesaurus concepts: Active galactic nuclei (16); Early universe (435); High-redshift galaxies (734)

1. Introduction

Until the launch of the James Webb Space Telescope (JWST), the earliest black holes known were a handful of extremely UV-luminous $z \approx 7$ quasars (e.g., Mortlock et al. 2011; Bañados et al. 2018; Matsuoka et al. 2018, 2023). While

[28] Hubble Fellow.

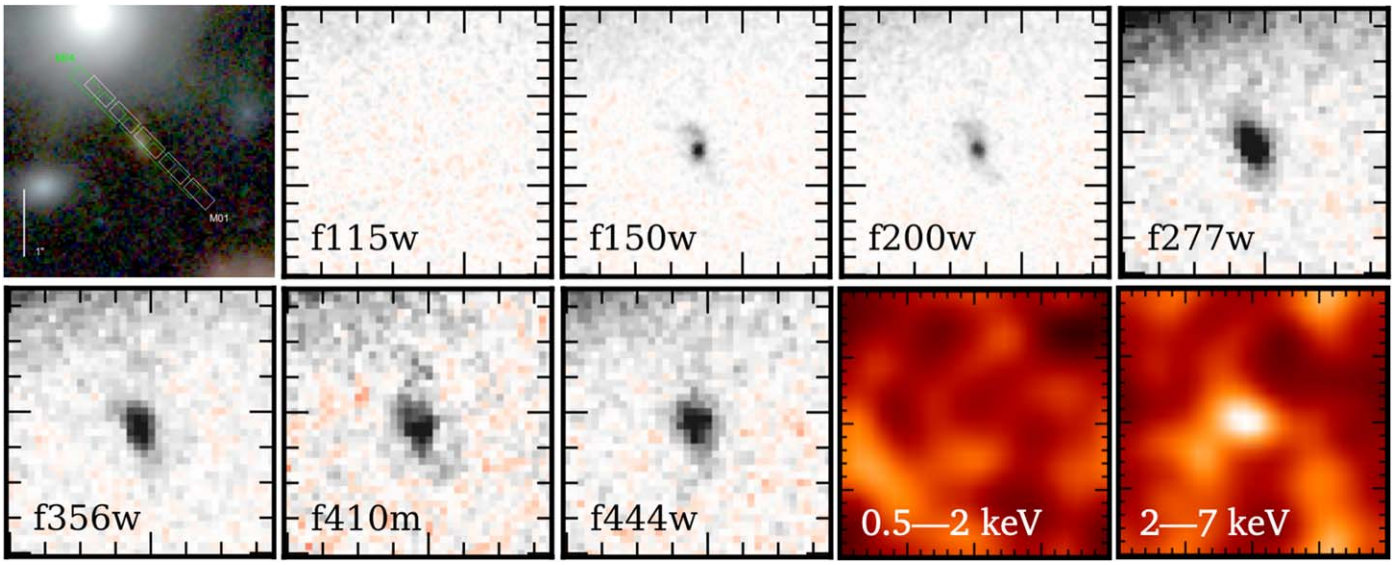

Figure 1. From top-left: NIRSpec/Prism MSA shutter positions for UHZ-1 (see Section 2), JWST/NIRCam images of UHZ-1 in filters F115W, F150W, F200W, F277W, F356, F410M, and F444W (photometric measurements from these calibrated data are presented in Figure 2) and Chandra X-ray images in the 0.5–2 and 2–7 keV bands (smoothed with a 1 pixel width Gaussian filter). JWST cutout images are $1\farcs5$ on a side, Chandra images are $5''$ on a side. These are oriented in standard North–East convention.

these sources are quite rare, given their high estimated masses, their existence leads to a timing challenge for the formation of supermassive black holes (SMBHs). If their initial seeds originate from the death of the first massive stars, with a typical remnant mass of $\sim 100\,M_{\odot}$ these black holes would need to accrete at or above the Eddington limit continuously for ~700–800 million years in order to reach the observed masses of $>10^9\,M_{\odot}$ (see Natarajan 2011; Fan et al. 2019, for a review). Theorists have therefore explored alternate seed formation models, with heavier seed BH mass functions ($\sim 10^4\,M_{\odot}$) that could form from the direct collapse of gas in the high-redshift Universe (see, for instance, Lodato & Natarajan 2006, 2007; Volonteri et al. 2008; Inayoshi et al. 2022). These heavy seeds are expected to be rare in general (e.g., Agarwal et al. 2013; Dayal et al. 2019; Habouzit et al. 2022), and their individual future growth trajectories are unclear. Therefore, it is unclear if UHZ-1 is a likely progenitor for the luminous optically detected Sloan Digital Sky Survey quasars. Guidance from cosmological simulations that track BH growth, the MASSIVE-BLACK suite in particular, have shown that the most massive BH at $z \sim 10$ does not necessarily grow to remain the most massive BH by $z = 6$ (Di Matteo et al. 2017, 2023). The details of the environment play an important role in shaping the accretion and, therefore, growth history of BHs.

The situation has gotten decidedly more interesting with the launch of JWST. A number of intriguing active galactic nuclei (AGN) candidates have been spectroscopically confirmed at more moderate luminosities (Kocevski et al. 2023; Matthee et al. 2023), with some discovered at $z > 7$ (Harikane et al. 2022; Furtak et al. 2023a; Larson et al. 2023; Maiolino et al. 2023a, 2023b). In the absence of other direct indicators of AGN activity (e.g., broadened Balmer emission lines), the most unambiguous identification of AGN activity is through the detection of high-energy X-ray emission. Due to the negative k-correction at X-ray energies, high-redshift AGN are preferentially detected at increasingly harder X-ray energies, making their identification more distinct from lower-energy X-rays produced by contaminating star formation emission.

Harnessing the exquisite spatial resolution afforded by the Chandra X-ray Observatory, the current record holder to date for the most distant ($z_{\rm phot} \sim 10.3$; Castellano et al. 2023) X-ray luminous AGN is UHZ-1, discovered behind the lensing cluster Abell 2744 (Bogdan et al. 2023). Previously identified as an extremely high-redshift candidate (Castellano et al. 2023), UHZ-1 is reported with a robust 4.2σ–4.4σ detection in the observed-frame 2–7 keV band with 20.6 net counts (Figure 1). At $z > 10$, these are extremely hard X-ray photons with rest-frame energies of $E \sim 22$–80 keV, which can only arise from an accreting BH. UHZ-1 is undetected in the softer 0.5–2 keV band, which the authors explain is likely due to UHZ-1 being heavily obscured with a Compton-thick column density of $N_{\rm H} \sim 10^{24}$–10^{25} cm^{-2}. Assuming their adopted lensing magnification of $\mu = 3.81$, and given the degeneracies related to the X-ray spectral fitting, the resultant intrinsic 2–10 keV X-ray luminosity is $L_{\rm X} \gtrsim 2 \times 10^{44}$ erg s^{-1}.

In this paper, we present the JWST/NIRSpec Prism spectroscopy confirming that UHZ-1 is at a redshift of $z = 10.07$ (Section 2). This deep spectrum was recently collected as part of the UNCOVER JWST treasury program (JWST-GO-2561; PIs: Labbe, Bezanson), which includes deep (~2.7–17 hr) low-resolution spectroscopy for ~700 JWST-selected targets. We further examine the rest-frame UV/optical spectral properties of UHZ-1 (Section 3), and estimate the stellar mass and star-formation rate (SFR) of the host galaxy (Section 4). Throughout, we assume a ΛCDM cosmology with $\Omega_M = 0.29$, $\Omega_\Lambda = 0.71$, and $H_0 = 69.6$ km s^{-1} Mpc^{-1}, with a Chabrier (2003) initial mass function (IMF).

2. JWST/NIRSpec Prism Spectroscopy of UHZ-1

2.1. MSA Observational Setup

UHZ-1 (Weaver et al. 2023), positioned at $\alpha = 3\overset{\circ}{.}567070796$, $\delta = -30\overset{\circ}{.}3778606$, was observed on 2023 July 31 and August 1 for a total of 7.1 hr as part of the multishutter array (MSA) follow-up program of the UNCOVER JWST field, Abell 2744 (Bezanson et al. 2022). The NIRSpec/Prism

observations of UNCOVER were split into seven MSA configurations, with UHZ-1 positioned on MSA 1 (2.7 hr) and 4 (4.4 hr) centered at $\alpha = 3.^{\circ}5839128$, $\delta = -30.^{\circ}3998611$ and $\alpha = 3.^{\circ}5586419$, $\delta = -30.^{\circ}3564066$, respectively. These observations employed a 2-POINT-WITH-NIRCam-SIZE2 dither pattern and a three-shutter slitlet nod pattern at an angle of V3PA $\sim 266.^{\circ}0$. MSA configuration 1 used the NRSIRS2-RAPID readout pattern, while MSA 4 used NRSIRS2. For further details of the observational setup see Bezanson et al. (2022) and S. H. Price et al. (2023, in preparation). Upon analysis it was determined that around the position of UHZ-1, MSA 1 suffered from an electrical short, and given the resultant low signal-to-noise, we do not use those data for any part of the analysis presented here. Hence, the total usable exposure time for UHZ-1 is 4.4 hr.

2.2. NIRSpec/Prism Data Reduction

The Prism spectra are reduced using msaexp (v0.6.10; Brammer 2022). Beginning from the level 2 products downloaded from MAST,[29] `msaexp` applies a correction for 1/f noise, identifies and masks snowballs, and removes the bias in each individual frame. Parts of the JWST science calibration and reduction pipeline (Bushouse et al. 2023) are used to apply World Coordinate System, identify, flat-field, and apply photometric corrections to each slit. 2D slits are then extracted and drizzled together onto a common grid. A local background subtraction is applied using vertically shifted, stacked 2D spectra. Finally, `msaexp` performs an optimal extraction using a Gaussian model to the collapsed spectrum with free center and width (e.g., Horne 1986). This work is based on an early (internal v0.3) spectroscopic reduction. We perform slit-loss corrections by applying a wavelength-independent calibration to scale the normalization of the spectrum to the photometry by convolving the single-mask extracted 1D spectra with the broad/medium band filters, comparing to the total photometry (Weaver et al. 2023), and modeling the wavelength-dependent linear correction with a first-order polynomial. Reduced data are planned for public release before Cycle 3 and presented in Price et al. (2023, in preparation.).

3. UHZ-1: A $z = 10.07$ X-Ray Luminous AGN

3.1. Prism Spectroscopy

The wide spectral coverage of the NIRSpec/Prism spectrum allows us to probe from the Lyman break all the way to ~4500 Å rest frame (Figure 2). Using `msaexp`, we fit stellar population and emission-line templates to the spectroscopy, and unambiguously confirm the redshift $z = 10.071 \pm 0.002$ with a strongly identified Lyman break and several emission lines. The previous best-fit photometric redshift solution for UHZ-1 was $z_{\rm phot} \sim 10.19 \pm 0.17$ produced using the EAZY (Brammer et al. 2008) package (see Atek et al. 2023), and $z_{\rm phot} \sim 10.87^{+0.21}_{-0.41}$ adapting the `Prospector`-β model (Johnson et al. 2021; Wang et al. 2023). The inset of Figure 2 presents the redshift probability functions produced by `msaexp` showing a narrow single-peaked P(z) at $z \sim 10.07$, which is consistent with the previous best-fit photometric redshift. We further verify the high-redshift nature of UHZ-1 using the publicly available Bayesian Analysis of Galaxies for Physical Inference and Parameter EStimation (`Bagpipes`; Carnall et al. 2018, 2019) code, finding a similar single-peaked redshift solution at $z = 10.068 \pm 0.003$. In addition to the strong blue UV/optical continuum with slope $\beta \sim -2.7$ (Castellano et al. 2023), we also note the presence of several weaker UV and optical lines, which we measure in the next section.

3.2. Spectral Emission Lines

We fit single Gaussians and low-order polynomial continua to all prominent emission lines, and present the emission-line centroids, fluxes, and signal-to-noise ratios in Table 1. We find significant detections of C III] λ1907, 1909, [Ne III] λ3869, and the [O II] λ3727, 3729 doublet (see Figure 3). Interestingly, despite the clear and robust X-ray detection of UHZ-1, and hence its identification as an AGN, we do not detect evidence for any broadened emission lines such as C IV or Mg II as expected for relatively unobscured AGN. Even for obscured AGN, typically high-equivalent-width, high-ionization narrow emission lines such as [Ne V]λ3426 are detected, which would point to the presence of a rapidly accreting BH. Instead, the only clear signature of AGN activity in this source comes from the strong detection of X-ray emission at hard energies. While lower-ionization lines such as [Ne III] can indicate the presence of an AGN, they are also readily produced by star formation, and this alone would not be the basis for an unambiguous AGN indicator (e.g., Goulding & Alexander 2009). The UV luminosity ($M_{\rm UV} \sim -19.85$) is also not distinctively high compared to similarly high-z star-forming galaxies. Taken together, the lack of obvious AGN emission lines and the clear detection of luminous hard X-ray emission, we can conclude that UHZ-1 is likely an extremely Compton-thick and optically obscured AGN, potentially similar to systems such as NGC 4945 in the local Universe (Matt et al. 2000; Yaqoob 2012).

4. Host-galaxy Properties

Based upon the nondetection of broadened emission lines as well as lack of prominent high-ionization lines and a blue UV continuum shape that is consistent with star formation, there is no clear and direct evidence for a significant contribution from the AGN to the UV/optical spectrum. Therefore, we can fit the spectrophotometry robustly, where the light contribution is dominated by the host galaxy, despite knowledge of the presence of an X-ray AGN.

We use the `Bagpipes` spectral energy distribution (SED) fitting code (Carnall et al. 2018, 2019) to perform this SED fit. We use Bruzual & Charlot (2003) stellar population models, the MILES spectral library (Sánchez-Blázquez et al. 2006; Falcón-Barroso et al. 2011), a Chabrier (2003) IMF, and Cloudy nebular emission models (Ferland et al. 2017). We utilize `PyMultinest` (Buchner et al. 2014; Feroz et al. 2019) to perform our sampling using the default `Bagpipes` convergence criteria. We parameterize the star formation history with a delayed-τ model (SFR $\propto te^{-t/\tau}$) with the age and τ as free parameters ($0.1\,{\rm Gyr} < {\rm age} < t_{\rm universe}$ and $0.01\,{\rm Gyr} < \tau < 5\,{\rm Gyr}$). We additionally allow the metallicity (with the stellar and gas phase metallicity fixed to the same value) and ionization parameter to vary, with $-2 < log(Z) < 0.3$ and $-3.5 < log(U) < -1.0$. We assume a Charlot & Fall (2000) dust model, with $0 < A_v < 5$ and $0.3 < n < 2.5$ as free parameters. We allow the redshift to vary around the best-

[29] Available from doi:10.17909/8k5c-xr27.

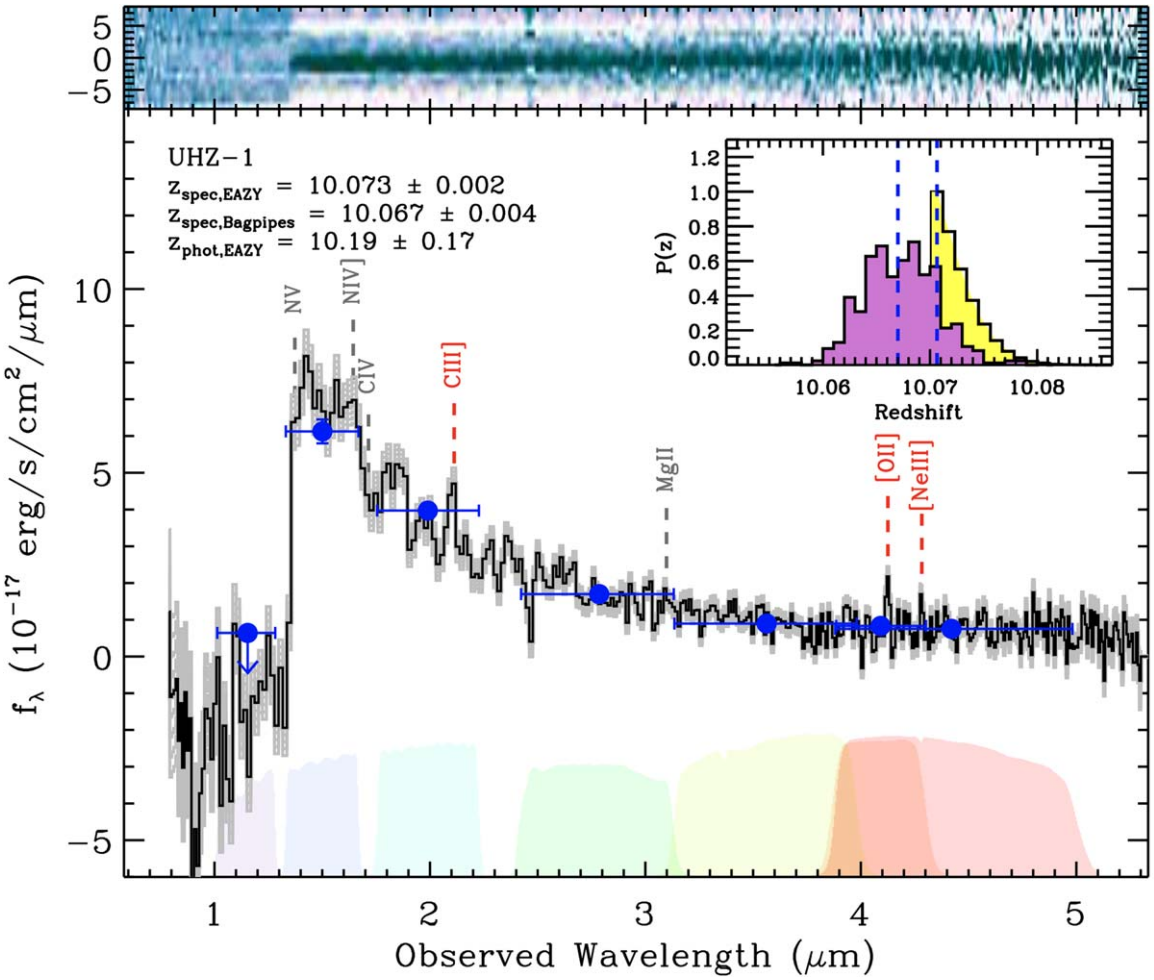

Figure 2. JWST/NIRSpec Prism spectroscopy of UHZ-1. Upper panel: 2D MSA Prism spectroscopy produced by `msaexp`. Lower panel: 1D spectral extraction in f_λ (in units of 10^{-17} erg s^{-1} cm^{-2} μm^{-1}) with associated statistical uncertainties (gray shaded region). Slit-loss corrections are defined by convolution of the JWST photometry with the Prism spectrum (see Section 2). Prominent and/or expected emission features are highlighted assuming $z_{spec} = 10.07$ with significant $>3\sigma$ detections and nondetections labeled in red and gray, respectively. Overlaid are the JWST/NIRCam photometry (blue circles) with associated filter responses highlighted. Inset panel: redshift probability distributions for fits to the NIRSpec spectroscopy produced by `EAZY` (yellow) and `BAGPIPES` (purple) packages.

Table 1
Emission-line Measurements of UHZ-1

Name	Obs. Cent. λ (μm)	Flux (10^{-20} erg s^{-1} cm^{-2})	S/N
NIV] λ1485	1.637	<112.40	<3
CIV $\lambda\lambda$1548, 1550	1.715	<99.04	<3
CIII] $\lambda\lambda$1907, 1909	2.101	67.93 ± 17.62	3.9
MgII λ2799	3.098	<30.03	<3
[OII] $\lambda\lambda$3727, 3729	4.124	29.29 ± 5.50	5.3
[NeIII] $\lambda\lambda$3869	4.282	14.63 ± 4.77	3.1

fitting spectroscopic redshift of 10.07 ± 0.05. Additionally, we apply the wavelength-dependent instrumental resolution curve to all models before fitting, assuming that the resolution is a nominal 1.3 times better than the preflight curve provided by STScI[30] (Curtis-Lake et al. 2023), and we leave the wavelength-independent velocity dispersion free between 1 and 2000 km s^{-1} as a nuisance parameter. We fit for a polynomial calibration vector of order 2 and the `Bagpipes`

[30] https://jwst-docs.stsci.edu/jwst-near-infrared-spectrograph/nirspec-instrumentation/nirspec-dispersers-and-filters

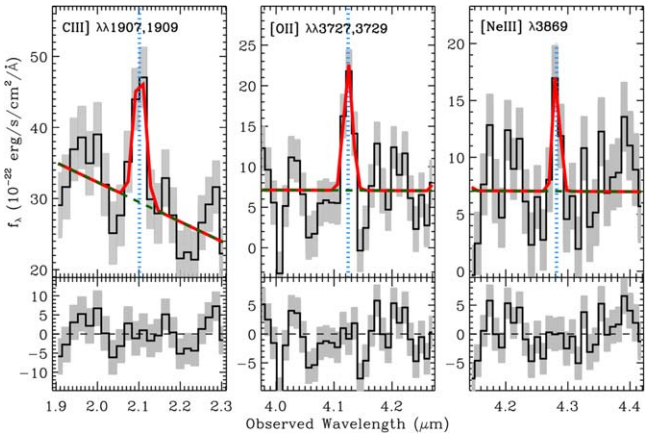

Figure 3. Upper panels: Gaussian line combined with low-order polynomial continua fits to the [C III] λ 1907, 1909, [O II] λ 3727, 3729 doublet, and [Ne III] λ 3869 emission features. Lower panels: residuals of the best fits.

white noise model to allow for underestimated errors up to a factor of 10. Finally, we place a signal-to-noise ceiling of 20 on both our photometry and spectroscopy to account for potential systematic issues with the flux calibration. We fit all available JWST/NIRCam (F115W/F150W/F200W/F277W/F356W/

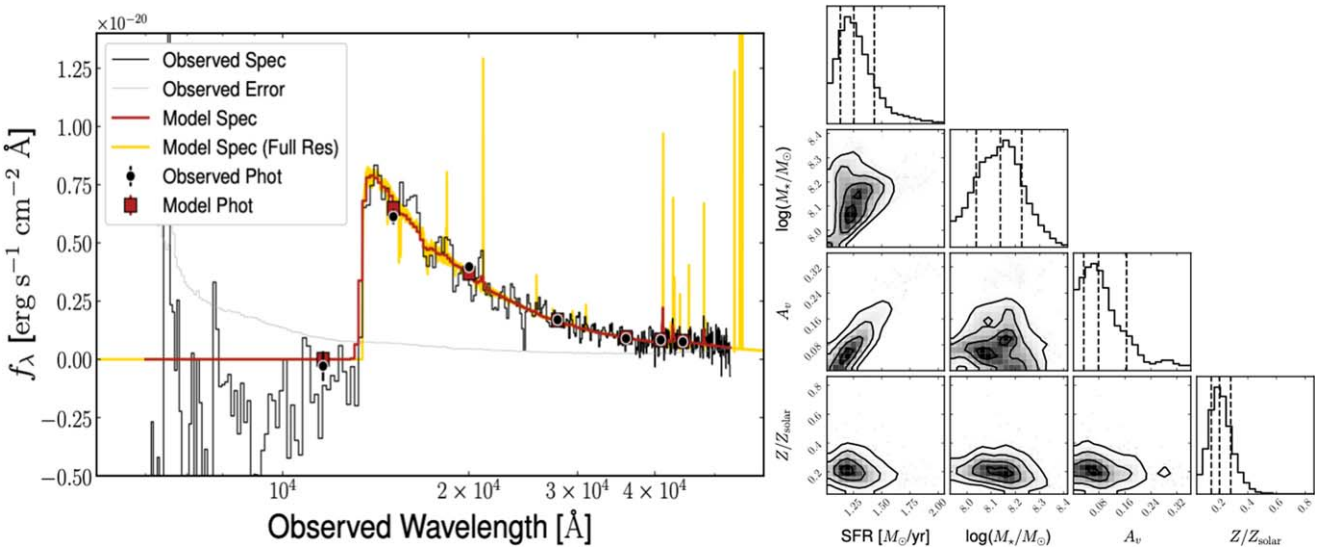

Figure 4. Stellar population synthesis modeling with `Bagpipes`. The left panel shows the observed galaxy SED and spectrum (black, showing only JWST photometry) after the application of the polynomial calibration with 1σ errors (assuming an error floor of 5%) and the median model (red). Additionally, the median model is shown at the full resolution (gold), highlighting the predicted emission features that are washed out by the instrumental resolution. In the right panel, we show the covariant posteriors for a number of key measured parameters after accounting for the magnification of the source.

Table 2
Host-galaxy Parameters

Parameter	Unit	Percentile		
		16th	50th	84th
SFR	$M_\odot$ yr^{-1}	1.13	1.25	1.43
$\log(M_\star/M_\odot)$	...	8.03	8.14	8.23
logU	⋯	−2.00	−1.78	−1.58
A_V	mag	0.03	0.08	0.16
t_{50}	Myr	45.1	64.9	96.6
Z	$Z_\odot$	0.15	0.20	0.28
$r_{\rm eff}$	arcsec	0.12	0.14	0.16
Sérsic n	⋯	0.79	1.06	1.64

F410M/F444W) and HST/ACS (F435W/F606W/F814W) and WFC3 (F105W/F125W/F160W) photometry in addition to the full NIRSPEC/Prism spectrum.

We present the best-fit model spectrum in Figure 4(a) along with the pairwise posterior distributions of relevant parameters in Figure 4(b), which have been corrected for the magnification of UHZ-1 with the median value of $\mu = 3.866$ ($\pm^{0.1}_{0.4}$; see Furtak et al. 2023b). The median, 16th, and 84th percentiles of the host-galaxy parameter posteriors are presented in Table 2. The magnification-corrected stellar mass of $\log(M_\star/M_\odot) = 8.1 \pm 0.1$ is fairly typical for $z \approx 10$ galaxies being spectroscopically confirmed with JWST (e.g., Curtis-Lake et al. 2023; Arrabal Haro et al. 2023), but is now more robustly constrained to the higher-mass end of the stellar mass previously inferred from photometry alone (Castellano et al. 2022; Bogdan et al. 2023) owing to the precise nature of the spectroscopic redshift in the `Bagpipes` fit. We note that fitting only the photometric data at the spectroscopic redshift of UHZ-1 produces a consistent measure of the stellar mass with $\log(M_\star/M_\odot) = 8.1 \pm 0.1$. The `Bagpipes` fit prefers an SFR of $\sim 1.3 \pm 0.2\ M_\odot\ {\rm yr}^{-1}$, i.e., an sSFR $\sim 10^{-8}$ yr^{-1}, which is similar to within a factor ∼2–3 of sSFR values inferred for galaxies of similar mass at this early epoch (e.g., Castellano et al. 2023). Finally, the fit prefers a moderately low stellar metallicity of $Z = 0.2 \pm 0.05$ compared to solar metallicity, similar to other early galaxies.

We perform a parametric Sérsic-profile fit to the NIRCam F444W image using `pysersic` (Pasha & Miller 2023), utilizing the NUTS sampler to explore the posterior (Hoffman & Gelman et al. 2014; Phan et al. 2019). We find the Sérsic index is consistent with $n \sim 1$, typical of disklike structures, and with an effective radius of $r_{\rm eff} \sim 0.14 \pm 0.02''$, which at $z = 10.07$ translates to a physical scale of $r_{\rm eff,physical} \sim 0.592$ kpc. We therefore find that UHZ-1 is also fairly typical in physical scales and extent measured for high-z galaxies in the GLASS field (Castellano et al. 2022).

5. Discussion and Summary

We have performed JWST NIRSpec/Prism spectroscopic follow-up of the $z \approx 10$ X-ray luminous AGN, UHZ-1, and confirm the highest-redshift (currently known) galaxy hosting an X-ray AGN, with a firm spectroscopic redshift of $z = 10.073 \pm 0.002$. The spectrum is likely dominated by host-galaxy light in the rest-frame UV/optical and stellar population synthesis analysis yields a stellar mass for the system of $\log M_* = 8.1 \pm 0.1\ M_\odot$. The size, mass, emission-line properties, and SFR of the host of UHZ-1 seem relatively typical of other known $z \approx 10$ galaxies. Here, we discuss the implications of UHZ-1 for the growth of supermassive BHs, and for their signatures in the very early Universe.

A large open question for the formation of supermassive black holes has been whether they originate from "light" or stellar-mass black holes, remnants from the death of massive stars ($\sim 100\ M_\odot$ seeds; Loeb & Rasio 1994; Bromm & Loeb 2003) or whether there are mechanisms that operate to form heavier initial seeds ($M_{\rm BH} \sim 10^3$–$10^5\ M_\odot$; Miller & Hamilton 2002; Portegies Zwart & McMillan 2002; Freitag et al. 2006; Devecchi & Volonteri 2009; Koushiappas et al. 2004; Lodato & Natarajan 2006, 2007; Alexander & Natarajan 2014; Begelman 2010; Natarajan et al. 2017; Natarajan 2021; Greene et al. 2020). As shown by Bogdan et al. (2023), to form the BH in UHZ-1 requires either

continuous growth exceeding the Eddington limit for >200 Myr, or a massive seed. Similar timing arguments have been made for UV-luminous quasars at $z > 6$; while they have more time to grow, they pose challenges for our current understanding of accretion models (e.g., Haiman & Loeb 2001; Natarajan 2011).

The ratio of BH mass to galaxy mass provides a complementary clue to the seeding mechanism. A key prediction of the heavy seed formation scenarios by the direct collapse of gas is that this ratio at early times, close to the seeding epoch, is significantly higher than found locally (Natarajan 2011; Natarajan et al. 2017). Heavy seeding models predict an early phase of overly massive BHs relative to the local $M_{\rm BH}/M_*$ relation (e.g., Natarajan et al. 2017). Under the assumption that the AGN is contributing little to the observed UV/optical continuum and emission lines, the measured host mass for UHZ-1 is roughly 0.5 dex higher with the benefit of spectroscopy compared to the median photometric value in Castellano et al. (2023). However, we still estimate a very high ratio of $M_{\rm BH}/M_*$ based on the X-ray emission. The X-ray source in UHZ-1 has an $L_{\rm X,int} \sim 2 \times 10^{44}$ erg s^{-1} (assuming $N_{\rm H} \sim 2 \times 10^{24}$ cm^{-2}), and an implied BH mass of $M_{\rm BH} \sim 10^{7-8}\ M_\odot$ conservatively assuming Eddington limited accretion and relevant uncertainties regarding the high Compton-thick column density observed in the X-rays (Bogdan et al. 2023). The implied BH-to-stellar-mass ratio in this system (combining relevant modeling uncertainties) based on our best-fit `Bagpipes` model is thus $M_{\rm BH}/M_{\rm gal} \approx 0.05$–$1.0$.

This BH is a much larger fraction of the galaxy mass than the typical ratio of ∼0.001–0.002 seen locally (Kormendy & Ho 2013; Reines & Volonteri 2015). At face value, this observation would strongly disfavor light-seed scenarios (in systems similar to UHZ-1), which typically result in BHs that are undermassive with respect to the host galaxy until the galaxy mass exceeds $\sim 10^{10}\ M_\odot$ Anglés-Alcázar et al. (2017); Catmabacak et al. (2022). Thus far, all luminous AGN discovered at $z > 5$ with estimates for both the BH mass and the galaxy mass have had high ratios, but this source is extreme even in that context (e.g., Izumi et al. 2019; Neeleman et al. 2021; Fan et al. 2023). This of course does not preclude a light-seed scenario concurrently taking place in other systems, particularly as such lower-mass BHs would be substantially more difficult to detect and may not be X-ray luminous (Natarajan 2021). However, the combination of the high BH mass, low galaxy mass at $z \sim 10$ and early accretion history modeling suggest that the particular BH in UHZ-1 was likely formed from a heavy seed (Natarajan et al. 2023). Indeed, given the extremely small volume probed by the UNCOVER region (∼40 arcmin^2), the number density of BHs formed from a heavy seed or a scenario involving light seeds that require substantial super-Eddington growth, cannot be vanishingly small with the detection of UHZ-1 and other systems thus far.

Despite the $>4\sigma$ detection in the 2–7 keV band (see Figure 1 and Bogdan et al. 2023), the lack of clear AGN signatures in the UV/optical given the luminous hard X-ray source present in this system is somewhat surprising. While highly unlikely given the precise locale and centroiding of the X-ray emission, it cannot be excluded that the X-ray association is coincidental. On the other hand, the lack of UV AGN signatures is not unusual. Even in other bona fide broad-line AGN detected by JWST, which interestingly lack X-ray emission despite their Type-1 AGN nature (e.g., Furtak et al. 2023c), these systems are also bereft of the typical broad and narrow AGN emission lines blueward of $H\beta$ (e.g., Harikane et al. 2023; Kocevski et al. 2023; Matthee et al. 2023; Labbe et al. 2023). Moreover, such objects are not entirely uncommon in the nearby Universe (e.g., NGC 1448; NGC 4945; see Alexander & Hickox 2012; Annuar et al. 2017) as even luminous AGN signatures can be swamped by strong star formation and/or extreme obscuration. Furthermore, the relatively high $L_{\rm X,int}/L_{\rm 1450,obs} \sim 0.7$ ratio also points toward a heavily buried AGN. Indeed, the relatively low $A_{\rm V} \sim 0.08$ mag suggests a low line-of-sight extinction to the galaxy, placing any obscuration on small nuclear scales, as suggested by the Compton-thick column measured in the X-rays. Longer-wavelength data may provide useful clues about the AGN's nature in UHZ-1. For example, due to the spectral coverage of the NIRSpec/Prism data, the current spectrum just misses the vital [O III] and Hβ complex (a typical diagnostic for AGN activity). Moreover, at significantly longer wavelengths, the rest-frame near and mid-IR wave bands can provide much cleaner information on the presence of AGN emission even in the most heavily obscured AGN due to the reemission by dust of the AGN signatures. Such wavelengths are fully accessible by JWST/MIRI out to rest-frame $\lambda < 2.5$ μm, giving access to the hot AGN dust continuum as well as high-ionization emission lines and the Paschen series. Indeed, the detection of lower-order Balmer lines and the Paschen series, given the lack of Balmer emission lines in the current NIRSpec/Prism data may point toward heavy obscuration in UHZ-1.

Objects such as UHZ-1 are only now beginning to be uncovered in the JWST data. The UNCOVER program hints at the power of deep NIRSpec spectroscopy to characterize the first growing black holes, while the high magnification ($\mu \sim 3.8 \pm 0.2$) certainly aids in the detection of objects such as that presented here. The detection of the unimpeded UV-photons produced due to star formation from UHZ-1 suggests that the obscuration of the growing BH is confined to the nuclear regions given the low inferred extinction along the line of sight. This suggests that at extremely high-redshift, even modest star-forming sources like UHZ-1, likely jump-started reionization. The number of AGN detected so far, given the relatively limited areas covered by JWST to date, suggests that an actively growing BH population may already be in place at this early epoch. However, because of the difficulty to detect the AGN signatures in UHZ-1, the further identification and characterization of the demographics of such systems may require a suite of diagnostics from JWST NIRCam, NIRSpec, MIRI, and in the X-rays.

Acknowledgments

The authors thank the anonymous referee for a constructive and insightful report that improved several aspects of the manuscript. A.D.G would like to thank M.A. Strauss for useful and enlightening conversations. A.D.G and J.E.G. acknowledge support from NSF/AAG grant No. 1007094. P.D. acknowledges support from the NWO grant 016.VIDI.189.162 ("ODIN") and the European Commission's and University of Groningen's CO-FUND Rosalind Franklin program. R.B. acknowledges support from the Research Corporation for Scientific Advancement (RCSA) Cottrell Scholar Award ID No: 27587. This work is based in part on observations made with the NASA/ESA/CSA James Webb Space Telescope. The data were obtained from the Mikulski Archive for Space

Telescopes at the Space Telescope Science Institute, which is operated by the Association of Universities for Research in Astronomy, Inc., under NASA contract NAS 5-03127 for JWST. The specific observations analyzed can be accessed via doi:10.17909/8k5c-xr27. These observations are associated with JWST Cycle 1 programs JWST-GO-2561 and JWST-ERS-1324. Support for program JWST-GO-2561 was provided by NASA through a grant from the Space Telescope Science Institute, which is operated by the Associations of Universities for Research in Astronomy, Incorporated, under NASA contract NAS5-26555. The Cosmic Dawn Center is funded by the Danish National Research Foundation (DNRF) under grant No. 140. Y.F. acknowledges support from NAOJ ALMA Scientific Research grant No. 2020-16B. Y.F. further acknowledges support from support from JSPS KAKENHI grant No. JP23K13149. H.A. and I.C. acknowledge support from CNES, focused on the JWST mission, and the Programme National Cosmology and Galaxies (PNCG) of CNRS/INSU with INP and IN2P3, cofunded by CEA and CNES. Á.B. acknowledges support from the Smithsonian Institution through NASA contract NAS8-03060. P.N. acknowledges support from the Gordon and Betty Moore Foundation and the John Templeton Foundation that fund the black hole Initiative (BHI) at Harvard University where she serves as one of the PIs. A.Z. acknowledges support by grant No. 2020750 from the United States-Israel Binational Science Foundation (BSF) and grant No. 2109066 from the United States National Science Foundation (NSF), and by the Ministry of Science & Technology, Israel.

ORCID iDs

Andy D. Goulding https://orcid.org/0000-0003-4700-663X
Jenny E. Greene https://orcid.org/0000-0002-5612-3427
David J. Setton https://orcid.org/0000-0003-4075-7393
Ivo Labbe https://orcid.org/0000-0002-2057-5376
Rachel Bezanson https://orcid.org/0000-0001-5063-8254
Tim B. Miller https://orcid.org/0000-0001-8367-6265
Hakim Atek https://orcid.org/0000-0002-7570-0824
Ákos Bogdán https://orcid.org/0000-0003-0573-7733
Gabriel Brammer https://orcid.org/0000-0003-2680-005X
Iryna Chemerynska https://orcid.org/0009-0009-9795-6167
Sam E. Cutler https://orcid.org/0000-0002-7031-2865
Pratika Dayal https://orcid.org/0000-0001-8460-1564
Yoshinobu Fudamoto https://orcid.org/0000-0001-7440-8832
Seiji Fujimoto https://orcid.org/0000-0001-7201-5066
Lukas J. Furtak https://orcid.org/0000-0001-6278-032X
Vasily Kokorev https://orcid.org/0000-0002-5588-9156
Gourav Khullar https://orcid.org/0000-0002-3475-7648
Joel Leja https://orcid.org/0000-0001-6755-1315
Danilo Marchesini https://orcid.org/0000-0001-9002-3502
Priyamvada Natarajan https://orcid.org/0000-0002-5554-8896
Erica Nelson https://orcid.org/0000-0002-7524-374X
Pascal A. Oesch https://orcid.org/0000-0001-5851-6649
Richard Pan https://orcid.org/0000-0002-9651-5716
Casey Papovich https://orcid.org/0000-0001-7503-8482
Sedona H. Price https://orcid.org/0000-0002-0108-4176
Pieter van Dokkum https://orcid.org/0000-0002-8282-9888
Bingjie Wang (王冰洁) https://orcid.org/0000-0001-9269-5046
John R. Weaver https://orcid.org/0000-0003-1614-196X
Katherine E. Whitaker https://orcid.org/0000-0001-7160-3632
Adi Zitrin https://orcid.org/0000-0002-0350-4488

References

Agarwal, B., Davis, A. J., Khochfar, S., Natarajan, P., & Dunlop, J. S. 2013, MNRAS, 432, 3438
Alexander, D. M., & Hickox, R. C. 2012, NewAR, 56, 93
Alexander, T., & Natarajan, P. 2014, Sci, 345, 1330
Anglés-Alcázar, D., Faucher-Giguère, C.-A., Quataert, E., et al. 2017, MNRAS, 472, L109
Annuar, A., Alexander, D. M., Gandhi, P., et al. 2017, ApJ, 836, 165
Arrabal Haro, P., Dickinson, M., Finkelstein, S. L., et al. 2023, ApJL, 951, L22
Atek, H., Chemerynska, I., Wang, B., et al. 2023, MNRAS, 524, 5486
Bañados, E., Venemans, B. P., Mazzucchelli, C., et al. 2018, Natur, 553, 473
Begelman, M. C. 2010, MNRAS, 402, 673
Bezanson, R., Labbe, I., Whitaker, K. E., et al. 2022, arXiv:2212.04026
Bogdan, A., Goulding, A., Natarajan, P., et al. 2023, arXiv:2305.15458
Brammer, G. 2022, msaexp: NIRSpec analyis tools, v0.3, Zenodo, doi:10.5281/zenodo.7299500
Brammer, G. B., van Dokkum, P. G., & Coppi, P. 2008, ApJ, 686, 1503
Bromm, V., & Loeb, A. 2003, ApJ, 596, 34
Bruzual, G., & Charlot, S. 2003, MNRAS, 344, 1000
Buchner, J., Georgakakis, A., Nandra, K., et al. 2014, A&A, 564, A125
Bushouse, H., Eisenhamer, J., Dencheva, N., et al. 2023, JWST Calibration Pipeline, v1.10.0, Zenodo, doi:10.5281/zenodo.7795697
Carnall, A. C., Leja, J., Johnson, B. D., et al. 2019, ApJ, 873, 44
Carnall, A. C., McLure, R. J., Dunlop, J. S., & Davé, R. 2018, MNRAS, 480, 4379
Castellano, M., Fontana, A., Treu, T., et al. 2022, ApJL, 938, L15
Castellano, M., Fontana, A., Treu, T., et al. 2023, ApJL, 948, L14
Çatmabacak, O., Feldmann, R., Anglés-Alcázar, D., et al. 2022, MNRAS, 511, 506
Chabrier, G. 2003, PASP, 115, 763
Charlot, S., & Fall, S. M. 2000, ApJ, 539, 718
Curtis-Lake, E., Carniani, S., Cameron, A., et al. 2023, NatAs, 7, 622
Dayal, P., Rossi, E. M., Shiralilou, B., et al. 2019, MNRAS, 486, 2336
Devecchi, B., & Volonteri, M. 2009, ApJ, 694, 302
Di Matteo, T., Angles-Alcazar, D., & Shankar, F. 2023, arXiv:2304.11541
Di Matteo, T., Croft, R. A. C., Feng, Y., Waters, D., & Wilkins, S. 2017, MNRAS, 467, 4243
Falcón-Barroso, J., Sánchez-Blázquez, P., Vazdekis, A., et al. 2011, A&A, 532, A95
Fan, X., Bañados, E., & Simcoe, R. A. 2023, ARA&A, 61, 373
Fan, X., Wang, F., Yang, J., et al. 2019, ApJL, 870, L11
Ferland, G. J., Chatzikos, M., Guzmán, F., et al. 2017, RMxAA, 53, 385
Feroz, F., Hobson, M. P., Cameron, E., & Pettitt, A. N. 2019, OJAp, 2, 10
Freitag, M., Gürkan, M. A., & Rasio, F. A. 2006, MNRAS, 368, 141
Furtak, L. J., Labbé, I., Zitrin, A., et al. 2023c, arXiv:2308.05735
Furtak, L. J., Zitrin, A., Plat, A., et al. 2023a, ApJ, 952, 142
Furtak, L. J., Zitrin, A., Weaver, J. R., et al. 2023b, MNRAS, 523, 4568
Goulding, A. D., & Alexander, D. M. 2009, MNRAS, 398, 1165
Greene, J. E., Strader, J., & Ho, L. C. 2020, ARA&A, 58, 257
Habouzit, M., Onoue, M., Bañados, E., et al. 2022, MNRAS, 511, 3751
Haiman, Z., & Loeb, A. 2001, ApJ, 552, 459
Harikane, Y., Ono, Y., Ouchi, M., et al. 2022, ApJS, 259, 20
Harikane, Y., Zhang, Y., Nakajima, K., et al. 2023, arXiv:2303.11946
Hoffman, M. D., Gelman, A., et al. 2014, J. Mach. Learn. Res., 15, 1593
Horne, K. 1986, PASP, 98, 609
Inayoshi, K., Onoue, M., Sugahara, Y., Inoue, A. K., & Ho, L. C. 2022, ApJL, 931, L25
Izumi, T., Onoue, M., Matsuoka, Y., et al. 2019, PASJ, 71, 111
Johnson, B. D., Leja, J., Conroy, C., & Speagle, J. S. 2021, ApJS, 254, 22
Kocevski, D. D., Onoue, M., Inayoshi, K., et al. 2023, ApJL, 945, L4
Kormendy, J., & Ho, L. C. 2013, ARA&A, 51, 511
Koushiappas, S. M., Bullock, J. S., & Dekel, A. 2004, MNRAS, 354, 292
Labbe, I., Greene, J. E., Bezanson, R., et al. 2023, arXiv:2306.07320
Larson, R. L., Finkelstein, S. L., Kocevski, D. D., et al. 2023, ApJL, 953, L29
Lodato, G., & Natarajan, P. 2006, MNRAS, 371, 1813
Lodato, G., & Natarajan, P. 2007, MNRAS, 377, L64
Loeb, A., & Rasio, F. A. 1994, ApJ, 432, 52
Maiolino, R., Scholtz, J., Curtis-Lake, E., et al. 2023a, arXiv:2308.01230
Maiolino, R., Scholtz, J., Witstok, J., et al. 2023b, arXiv:2305.12492
Matsuoka, Y., Onoue, M., Iwasawa, K., et al. 2023, ApJL, 949, L42
Matsuoka, Y., Strauss, M. A., Kashikawa, N., et al. 2018, ApJ, 869, 150
Matt, G., Fabian, A. C., Guainazzi, M., et al. 2000, MNRAS, 318, 173
Matthee, J., Naidu, R. P., Brammer, G., et al. 2023, arXiv:2306.05448
Miller, M. C., & Hamilton, D. P. 2002, MNRAS, 330, 232

Mortlock, D. J., Warren, S. J., Venemans, B. P., et al. 2011, Natur, 474, 616
Natarajan, P. 2011, BASI, 39, 145
Natarajan, P. 2021, MNRAS, 501, 1413
Natarajan, P., Pacucci, F., Ferrara, A., et al. 2017, ApJ, 838, 117
Natarajan, P., Pacucci, F., Ricarte, A., et al. 2023, arXiv:2308.02654
Neeleman, M., Novak, M., Venemans, B. P., et al. 2021, ApJ, 911, 141
Pasha, I., & Miller, T. B. 2023, arXiv:2306.05454
Phan, D., Pradhan, N., & Jankowiak, M. 2019, arXiv:1912.11554
Portegies Zwart, S. F., & McMillan, S. L. W. 2002, ApJ, 576, 899
Reines, A. E., & Volonteri, M. 2015, ApJ, 813, 82
Sánchez-Blázquez, P., Peletier, R. F., Jiménez-Vicente, J., et al. 2006, MNRAS, 371, 703
Volonteri, M., Lodato, G., & Natarajan, P. 2008, MNRAS, 383, 1079
Wang, B., Leja, J., Bezanson, R., et al. 2023, ApJL, 944, L58
Weaver, J. R., Cutler, S. E., Pan, R., et al. 2023, arXiv:2301.02671
Yaqoob, T. 2012, MNRAS, 423, 3360